INTERNATIONAL ATOMIC ENERGY AGENCY
UNITED NATIONS EDUCATIONAL, SCIENTIFIC AND CULTURAL ORGANIZATION
INTERNATIONAL CENTRE FOR THEORETICAL PHYSICS
I.C.T.P., P.O. BOX 586, 34100 TRIESTE, ITALY, CABLE: CENTRATOM TRIESTE

SMR.769 -8

WORKSHOP ON "NON-LINEAR ELECTROMAGNETIC INTERACTIONS IN SEMICONDUCTORS"

1 - 10 AUGUST 1994

"Stable States in Surface Emitting Semiconductor Lasers"

F. PRATI
Dipartimento di Fisica
Universita' di Milano
Via Celoria 16
20133 Milano
Italy

Stable States in Surface Emitting Semiconductor Lasers

F. Prati, A. Tesei, L. A. Lugiato
Dipartimento di Fisica dell' Universitá di Milano
via Celoria 16, 20133 Milano, Italy

R. J. Horowicz
Departamento de Fisica, Pontificia Universidade Catolica de Rio de Janeiro
Marques S. Vicente 225, Rio de Janeiro, Brasil

Abstract – We consider a vertical cavity surface emitting semiconductor laser which operates with two frequency-degenerate doughnut modes, and combinations thereof. We identify a small region in the parameter space, where there is bistability between the two doughnut states, and another domain in which the TEM_{10} mode, and all the configuration obtained from it by rotation around the laser axis, are stable. The degeneracy by rotation can be eliminated by considering a pump region of square section; in this case there is bistability between two stationary states, in which the two intensity peaks are located along the diagonals of the square. In all the rest of the parameter space the system exhibits dynamical oscillations.

1 Introduction

The field of Transverse Nonlinear Optics (see e. g. [1- 3] and references quoted therein), which studies the spontaneous formation and transformation of spatiotemporal patterns in optical systems, showed in the last decade an impressive development linked to the issues of fundamental interest raised by these investigations. However, up to now the effort to exploit these results in the direction of practical applications remained limited. For example, the possibility of controlling a one-dimensional array of spatial solitons [4] by appropriate use of spatial modulation has been numerically demonstrated [5]. The dynamics of switching between spatial solitons has also been investigated [6]. The use of a laser, operating in a regime of spatial multistability [7] as a decision element in an optical associative memory has been described [8,9]. The control of transverse-wave interactions in nonlinear passive optical systems with 2D feedback [10] and the realization of an optical design kit for nonlinear spatial dynamics [11] have been shown theoretically and experimentally.

A recent paper [12] reports theoretical and experimental results which demonstrate the possibility of low energy switching in a bistable laser operating with two doughnut modes. Most interesting is a numerical simulation with a two-level model for values of parameters compatible with the case of surface-emitting lasers [13-16]; the results indicate the possibility of obtaining the transition from one to the other doughnut state by a switching energy on the order of some femtojoules [12]. However these simulations did not include an important ingredient, namely the linewidth factor [17,18] which constitutes the main element of difference between semiconductor lasers and the two-level model. Because the formation of transverse structures in lasers is very sensitive to the phase effects, it may be anticipated that the inclusion of the linewidth factor is necessary in order to obtain a correct understanding of the behaviour of spatially multistable semiconductor lasers. Actually, the importance of this factor in the generation of transverse modulation instability has been already evidenced in the case of broad-area semiconductor lasers [19].

The aim of this paper is just to analyze in details the effects which arise from the linewidth factor. Precisely, we consider a surface-emitting semiconductor laser (SEL) in such conditions that it operates only with two frequency-degenerate doughnut modes (the possibility of emission of doughnut-shaped fields in SEL has been experimentally demonstrated [14-16]) or, equivalently, with the two modes TEM_{10} and TEM_{01} , and combinations thereof (two-peak solutions). We perform an analytical study of the stationary states and of their stability, and simulate numerically the behaviour of the system in those ranges of parameters for which no stable stationary solution exists. We consider both the standard case of cylindrically symmetric and that of square-shaped active region.

In Sec. 2 we introduce the model and compare it with that for a two-level system. The stability of the doughnut and two-peak solutions is studied in Sec. 3 in the case of cylindrical symmetry. In Sec. 4 the effects of a square configuration are analyzed. The concluding Sec. 5 summarizes and discusses the main results of the paper.

2 Description of the model

We consider a cylindrical cavity SEL of length L and diameter d (Fig. 1). The crystal contains a thin active region of width $L_A \ll L$. We will consider both the case of circular (Fig. 2a) and square (Fig. 2b) transverse section of the active region: d_A will denote the diameter of the circle and l_A the length of the side of the square. The reflectivity at the two facets of the crystal is R.

If the structure of the laser is weakly index-guided, the electric field is very nearly linearly polarized [20] and the propagation equation can be cast in the scalar form

$$\nabla^2 \mathcal{E} - \mu_0 \epsilon(r) \frac{\partial^2 \mathcal{E}}{\partial t^2} = \frac{1}{\epsilon_0 c^2} \frac{\partial^2 \mathcal{P}}{\partial t^2} \tag{1}$$

where μ_0, ϵ_0 and c are the magnetic permeability, the dielectric constant and the velocity of light in free space, respectively, and $\epsilon(r)$ is the background dielectric constant in the medium. Because of the geometry of the system we adopt cylindrical coordinates (ρ, φ, z): z is the direction of propagation of light and the Laplacian is

$$\nabla^2 = \nabla_\perp^2 + \frac{\partial^2}{\partial z^2}, \qquad \nabla_\perp^2 = \frac{\partial^2}{\partial r^2} + \frac{1}{r}\frac{\partial}{\partial r} + \frac{1}{r^2}\frac{\partial^2}{\partial \varphi^2}. \tag{2}$$

In order to study the modes of the cavity we can make reference to the results relative to graded-index fibers. It is well-known that the modes of a fiber, whose index profile can be approximated by a power law, are very similar in shape to the Gauss-Laguerre modes of a resonator with spherical mirrors [21]. This result becomes exact in the case of parabolic profile of the refractive index. We will then assume that the dielectric constant $\epsilon(r)$ varies according to the law

$$\epsilon(r) = \epsilon(0)\left(1 - \frac{r^2}{h^2}\right), \tag{3}$$

with $h \gg d$.

Correspondingly the transverse profile of the refractive index $n(r)$ is

$$n(r) = n(0)\sqrt{1 - \frac{r^2}{h^2}} \tag{4}$$

where $n(0) = c\sqrt{\mu_0 \epsilon(0)}$ is the refractive index on the laser axis. In the limit $h \gg d$ one has $n(d/2) \simeq n(0)$: the laser is weakly index-guided.

The above model is rather idealized because it describes a medium whose refractive index decreases parabolically from $n(0)$ and eventually becomes negative for $r > h$. Nevertheless, in the region of physical interest $r \leq d/2$, Eqs. (3) and (4) make sense. The advantage of this crude model is that it allows for a simple description of the cavity modes as Gauss-Laguerre modes. It must be noted that more realistic models [20] lead to solutions that, under appropriate conditions, can be approximated very well by Gauss-Laguerre functions, even if they must be expressed in terms of Bessel functions.

In the slowly varying envelope and paraxial approximations we write

$$\mathcal{E} = \mathcal{E}_0 e^{-i\omega_0 t} + c.c. = \left[E(r,\varphi,z,t)e^{ik_0 z} + B(r,\varphi,z,t)e^{-ik_0 z}\right] e^{-i\omega_0 t} + c.c. \tag{5}$$

$$\mathcal{P} = \mathcal{P}_0 e^{-i\omega_0 t} + c.c. = \left[P_E(r,\varphi,z,t)e^{ik_0 z} + P_B(r,\varphi,z,t)e^{-ik_0 z}\right] e^{-i\omega_0 t} + c.c. \tag{6}$$

where E and B represent the forward and backward electric field, respectively, and $k_0 = \omega_0 n(0)/c$ is the wave vector of a wave of frequency ω_0 propagating in a homogeneous medium with refractive index $n(0)$.
The electric field $\mathcal{E}_0$ and the induced polarization $\mathcal{P}_0$ are linked by the relation

$$\mathcal{P}_0 = \epsilon_0 \chi(N) \mathcal{E}_0 \,, \tag{7}$$

which implies

$$P_E = \epsilon_0 \chi(N) E \qquad\qquad P_B = \epsilon_0 \chi(N) B \,. \tag{8}$$

If we assume linear gain, the susceptibility $\chi(N)$ is defined as [22]

$$\chi(N) = -\frac{n(r)c}{\omega_0} (\alpha + \mathrm{i})\, a(N - N_0) \tag{9}$$

where α is the linewidth enhancement factor [17], N is the carrier density, N_0 is the transparency value and a is the phenomenological gain coefficient ($N_0 = 3{\cdot}10^{18}$ cm^{-3}, $a = 3 \cdot 10^{-16}$ cm^2 for GaAlAs/GaAs systems [13]).

Taking into account Eqs. (5-9), we obtain the following propagation equations for the slowly varying envelopes E and B

$$\frac{1}{2\mathrm{i}k_0}\left(\nabla_\perp^2 - \frac{k_0^2 r^2}{h^2}\right) E + \frac{\partial E}{\partial z} + \frac{1}{v}\left(1 - \frac{r^2}{h^2}\right)\frac{\partial E}{\partial t} = \frac{a}{2}\sqrt{1 - \frac{r^2}{h^2}}(1 - \mathrm{i}\alpha)(N - N_0)E \tag{10}$$

$$\frac{1}{2\mathrm{i}k_0}\left(\nabla_\perp^2 - \frac{k_0^2 r^2}{h^2}\right) B - \frac{\partial B}{\partial z} + \frac{1}{v}\left(1 - \frac{r^2}{h^2}\right)\frac{\partial B}{\partial t} = \frac{a}{2}\sqrt{1 - \frac{r^2}{h^2}}(1 - \mathrm{i}\alpha)(N - N_0)B \tag{11}$$

where $v = c/n(0)$.

2.1 Eigenmodes of the cavity

The eigenmodes of the cavity are the solutions of the equations obtained from Eqs. (10) and (11) by setting $a = 0$ and $\partial E/\partial t = \partial B/\partial t = 0$. Restricting our analysis to the forward field we have

$$\left(\nabla_\perp^2 - \frac{k_0^2 r^2}{h^2}\right) E = -2\mathrm{i}k_0 \frac{\partial E}{\partial z} \tag{12}$$

which, by defining the normalized radial coordinate

$$\rho = \frac{r}{w_0} \,, \qquad\qquad w_0 = \sqrt{\frac{2h}{k_0}} \,, \tag{13}$$

becomes

$$\left(\frac{1}{4}\nabla_\perp'^2 - \rho^2\right) E = -\mathrm{i}h \frac{\partial E}{\partial z} \,, \tag{14}$$

where $\nabla_\perp'^2$ is the transverse Laplacian in the (ρ, φ) variables.
We now introduce the Gauss-Laguerre modes defined as

$$A_{p,l}(\rho, \varphi) = \sqrt{\frac{2}{\pi}} (2\rho^2)^{|l|/2} \left[\frac{p!}{(p + |l|)!}\right]^{1/2} L_p^{|l|}(2\rho^2) \mathrm{e}^{-\rho^2}\, \mathrm{e}^{\mathrm{i}l\varphi} \,, \tag{15}$$

where $p = 0, 1, 2 \ldots$, $l = 0, \pm 1, \pm 2 \ldots$ and $L_p^{|l|}$ are the generalized Laguerre polynomials. The functions $A_{p,l}$ are the eigenmodes of a resonator with spherical mirrors in the limit $z \ll z_0$, where z_0 is the Rayleigh length [23]. They form a complete set in the plane (ρ, φ), obey the orthonormality relation

$$\int_0^{2\pi} d\varphi \int_0^{\infty} d\rho\rho \; A^*_{p,l}(\rho,\varphi) A_{p',l'}(\rho,\varphi) = \delta_{p,p'}\delta_{l,l'} \tag{16}$$

and are solutions of the equation

$$\left(\frac{1}{4}\nabla_\perp'^2 - \rho^2\right) A_{p,l} = -(2p + |l| + 1) A_{p,l} \; . \tag{17}$$

Comparing Eq. (17) with Eq. (14) it is evident that the latter admits solutions of the form

$$E(\rho,\varphi,z) = \mathcal{A}_{p,l}(\rho,\varphi,z) = A_{p,l}(\rho,\varphi) \mathrm{e}^{-\mathrm{i}(2p+|l|+1)z/h} \; . \tag{18}$$

The functions $\mathcal{A}_{p,l}(\rho,\varphi,z)$ are the eigenmodes of a cavity containing a medium with parabolic index profile. They are very similar to the Gauss-Laguerre modes of a resonator with spherical mirrors [23]. The main differences are

i) The beam waist w_0 of the modes $\mathcal{A}_{p,l}$ is independent from z.

ii) The role of the Rayleigh length here is played by the parameter h

$$h = \frac{k_0 w_0^2}{2} \; . \tag{19}$$

It can be easily checked that the functions $\mathcal{A}_{p,l}(\rho,\varphi,-z)$ are the solutions of the equation for the backward field B.

The eigenfrequency of the mode with longitudinal index m and transverse indices p and l is

$$\omega_{mpl} = \frac{v}{L}\pi m + \frac{v}{h}(2p + |l| + 1) \; . \tag{20}$$

As in the case of a resonator with spherical mirrors the modes gather in degenerate families of index $q = 2p + |l|$ consisting of $q + 1$ modes. The frequency separation is

$$\Delta\omega_L = \frac{v}{L}\pi \tag{21}$$

for longitudinal modes and

$$\Delta\omega_T = \frac{v}{h} \tag{22}$$

for transverse modes. In the case of weakly index-guided lasers $L \simeq d \ll h$ the ratio $\Delta\omega_T/\Delta\omega_L = L/h\pi$ is much smaller than 1, and the eigenfrequencies spectrum is similar to that of a quasi-planar resonator.

Hereafter we will choose the frequency of the fundamental Gaussian mode with fixed longitudinal index $\overline{m}$ as reference frequency

$$\omega_0 = \omega_{\overline{m}00} \; . \tag{23}$$

Finally, it is worth noting that, if the region occupied by the modes is comparable with the size of the laser one has, for a weakly index guided structure,

$$w_0 \ll h \; , \tag{24}$$

and therefore, using Eq. (13),

$$k_0 h \gg 1 \,. \tag{25}$$

We observe that the last condition, which will be used in the following to simplify the dynamical equation, is necessary to justify the slowly varying envelope approximation. In fact, such an approximation requires that the exponential factor in Eq. (18) varies much more slowly than $\exp(\mathrm{i}k_0 z)$.

2.2 Dynamical equations

Let us come back to the equations which include the effects of the active region. After the transformations introduced in the previous section we have from Eqs. (10) and (11)

$$\frac{1}{\mathrm{i}h}\left(\frac{1}{4}\nabla_\perp'^2 - \rho^2\right)E + \frac{\partial E}{\partial z} + \frac{1}{v}\left(1 - \frac{2\rho^2}{k_0 h}\right)\frac{\partial E}{\partial t} = \frac{a}{2}\sqrt{1 - \frac{2\rho^2}{k_0 h}}(1 - \mathrm{i}\alpha)(N - N_0)E \,, \tag{26}$$

$$\frac{1}{\mathrm{i}h}\left(\frac{1}{4}\nabla_\perp'^2 - \rho^2\right)B - \frac{\partial B}{\partial z} + \frac{1}{v}\left(1 - \frac{2\rho^2}{k_0 h}\right)\frac{\partial B}{\partial t} = \frac{a}{2}\sqrt{1 - \frac{2\rho^2}{k_0 h}}(1 - \mathrm{i}\alpha)(N - N_0)B \,. \tag{27}$$

We observe that, because of condition (25), the terms $2\rho^2/k_0 h$ can be neglected with respect to 1. Then to be consistent with our approximations the appropriate equations for E and B in the slowly varying envelope approximation are

$$\frac{1}{\mathrm{i}h}\left(\frac{1}{4}\nabla_\perp'^2 - \rho^2\right)E + \frac{\partial E}{\partial z} + \frac{1}{v}\frac{\partial E}{\partial t} = \frac{a}{2}(1 - \mathrm{i}\alpha)(N - N_0)E \,, \tag{28}$$

$$\frac{1}{\mathrm{i}h}\left(\frac{1}{4}\nabla_\perp'^2 - \rho^2\right)B - \frac{\partial B}{\partial z} + \frac{1}{v}\frac{\partial B}{\partial t} = \frac{a}{2}(1 - \mathrm{i}\alpha)(N - N_0)B \,. \tag{29}$$

The set of dynamical equations is completed by the rate equation for the carrier density N

$$\frac{\partial N}{\partial t} = \frac{I}{q_e V} - \frac{N}{\tau_r} - av\frac{\epsilon(0)|\mathcal{E}_0|^2}{2\hbar\omega_0}(N - N_0) + \tilde{D}\nabla'^2 N \tag{30}$$

where I is the injected current, q_e is the electron charge, V is the active volume, τ_r is the recombination time and $\tilde{D}$ is the diffusion coefficient. In this equation av represent the gain coefficient per unit of time while $\epsilon(0)|\mathcal{E}_0|^2/2\hbar\omega_0$ is the photon density, and we assume that the dielectric constant in the medium is constant and equal to $\epsilon(0)$.
Eq. (30) is complicated because of the presence of the diffusion term. However, the main effect of a sizable diffusion is to wash out the grating effects which arise from the standing wave structure of the electric field. Therefore, it is reasonable to neglect the diffusion term and simultaneously assume that N exhibits no grating structure [22]. In this approximation the dynamics of N is ruled by the simpler equation

$$\frac{\partial N}{\partial t} = \frac{I}{q_e V} - \frac{N}{\tau_r} - av\frac{\epsilon(0)}{2\hbar\omega_0}\Gamma(|E|^2 + |B|^2)(N - N_0) \,, \tag{31}$$

where Γ is the confinement factor which represents the fraction of mode energy confined in the active region of volume V.
By introducing the scaled quantities

$$I_0 = \frac{q_e V N_0}{\tau_r}, \qquad g = \frac{aN_0}{2}\left(\frac{I}{I_0} - 1\right)$$

$$\overline{E} = \sqrt{\frac{\epsilon(0)\tau_r a v \Gamma}{\hbar\omega_0}}\, E, \qquad \overline{B} = \sqrt{\frac{\epsilon(0)\tau_r a v \Gamma}{\hbar\omega_0}}\, B, \qquad \overline{D} = \frac{N/N_0 - 1}{I/I_0 - 1}$$

the dynamical equations describing the laser become

$$\frac{1}{\mathrm{i}h}\left(\frac{1}{4}\nabla_\perp'^2 - \rho^2\right)\overline{E} + \frac{\partial\overline{E}}{\partial z} + \frac{1}{v}\frac{\partial\overline{E}}{\partial t} = g(1-\mathrm{i}\alpha)\overline{D}\,\overline{E}\,, \tag{32}$$

$$\frac{1}{\mathrm{i}h}\left(\frac{1}{4}\nabla_\perp'^2 - \rho^2\right)\overline{B} - \frac{\partial\overline{B}}{\partial z} + \frac{1}{v}\frac{\partial\overline{B}}{\partial t} = g(1-\mathrm{i}\alpha)\overline{D}\,\overline{B}\,, \tag{33}$$

$$\frac{\partial\overline{D}}{\partial t} = -\frac{1}{\tau_r}\left[\overline{D}\left(1 + \frac{|\overline{E}|^2 + |\overline{B}|^2)}{2}\right) - \chi_V\right] \tag{34}$$

where χ_V is the characteristic function of the active region

$$\chi_V(\rho,\varphi,z) = \begin{cases} 1 & \text{in } V \\ 0 & \text{outside } V \end{cases}\,. \tag{35}$$

At this point we expand the slowly varying envelopes $\overline{E}$ and $\overline{B}$ in terms of the eigenmodes $\mathcal{A}_{pl}$ of the cavity

$$\overline{E} = \sum_{p,l} \mathcal{A}_{pl}(\rho,\varphi,z)\; e_{pl}(z,t) \tag{36}$$

$$\overline{B} = \sum_{p,l} \mathcal{A}_{pl}(\rho,\varphi,-z)\; b_{pl}(z,t)\,. \tag{37}$$

The mode amplitudes e_{pl} and b_{pl} are solutions of the equations

$$\frac{\partial e_{pl}}{\partial z} = -\frac{1}{v}\frac{\partial e_{pl}}{\partial t} + g(1-\mathrm{i}\alpha)\int_0^{2\pi} d\varphi \int_0^\infty d\rho\rho\; \mathcal{A}^*_{pl}(z)\overline{D}\,\overline{E} \tag{38}$$

$$-\frac{\partial b_{pl}}{\partial z} = -\frac{1}{v}\frac{\partial b_{pl}}{\partial t} + g(1-\mathrm{i}\alpha)\int_0^{2\pi} d\varphi \int_0^\infty d\rho\rho\; \mathcal{A}^*_{pl}(-z)\overline{D}\,\overline{B} \tag{39}$$

and they obey the boundary conditions

$$e_{pl}(0,t) = \sqrt{R}\; b_{pl}(0,t) \tag{40}$$

$$b_{pl}(L,t) = \sqrt{R}\; e_{pl}(L,t)\mathrm{e}^{-\mathrm{i}\delta_{pl}} \tag{41}$$

where

$$\delta_{pl} = \frac{\omega_{\overline{m}pl} - \omega_{\overline{m}00}}{v/2L} = \frac{2L}{h}(2p + |l|)\,. \tag{42}$$

We observe that for GaAlAs/GaAs systems the gain per unit of length is $g \simeq 10^3$ cm^{-1}, while typical values for the length of the active region L_A and the reflectivity R in a vertical cavity SEL are $L_A \simeq 10^{-5}$ cm and $R = 0.99$ [16]. Moreover, for a weakly index-guided laser, $L \ll h$ and, taking into account Eq. (42), one has $\delta_{pl} \ll 1$ for all the modes belonging to families of order $q = 2p + |l|$ not too high. Therefore we can assume the uniform field limit

$$gL_A \ll 1, \qquad |\ln R| \ll 1, \tag{43}$$

$$C = \frac{gL_A}{|\ln R|}, \qquad a_{pl} = \frac{\delta_{pl}}{|\ln R|} \qquad \text{of order unity} \tag{44}$$

where $2C$ and a_{pl} are the pump parameter and the cavity detuning parameter for mode p, l, respectively.
Following the same steps as in [24] with slight changes due to the fact that here we are considering a Fabry-Perot cavity instead of a ring resonator, we define the new modal amplitudes

$$\varphi_{pl}(z,t) = \exp\left[\frac{1}{2}\left(\frac{z}{L}-1\right)\ln R - \mathrm{i}\frac{z}{2L}\delta_{pl}\right] e_{pl}(z,t) \tag{45}$$

$$\psi_{pl}(z,t) = \exp\left[-\frac{1}{2}\frac{z}{L}\ln R + \mathrm{i}\frac{z}{2L}\delta_{pl}\right] b_{pl}(z,t) \tag{46}$$

which obey the periodic boundary conditions

$$\varphi_{pl}(0,t) = \psi_{pl}(0,t) \tag{47}$$

$$\varphi_{pl}(L,t) = \psi_{pl}(L,t) \tag{48}$$

and in the limit of Eqs. (43-44) are nearly uniform along z and nearly equal to each other in the active region. We then introduce the averaged quantities

$$f_{pl}(t) = \frac{1}{L}\int_0^L dz\varphi_{pl}(z,t) \simeq \frac{1}{L}\int_0^L dz\psi_{pl}(z,t) \tag{49}$$

$$D(\rho,\varphi,t) = \frac{1}{L}\int_0^L dz\overline{D}(\rho,\varphi,z,t) \tag{50}$$

and we set in the dynamical equations the averages of products equal to the products of the averages (again, due to the quasi uniformity of φ_{pl}, ψ_{pl} and $\overline{D}$). The final equations are

$$\frac{df_{pl}}{d\tau} = -(1+\mathrm{i}a_{pl})f_{pl} + 2C(1-\mathrm{i}\alpha)\int_0^{2\pi}d\varphi\int_0^{\infty}d\rho\rho\; A_{pl}^{*}\, D\, F \tag{51}$$

$$\frac{\partial D}{\partial\tau} = -\gamma\left[D(1+|F|^2) - \chi_V\right] \tag{52}$$

where

$$F(\rho,\varphi,t) = \sum_{pl} A_{pl}(\rho,\varphi)f_{pl}(t), \tag{53}$$

$$\tau = kt, \qquad \gamma = \frac{1}{k\tau_r}, \qquad k = \frac{v}{L}\frac{|\ln R|}{2}. \tag{54}$$

As shown in the Appendix, these equations are completely equivalent to the equations for a detuned two-level Class-B laser, where the role of the linewidth enhancement factor α is played by the atomic detuning. Therefore, all the results of the next sections apply to such kind of lasers, too.
It is worth noting that the cavity detuning parameters a_{pl} depend on the transverse indices p and l only via the combination $2p+|l|$ and

$$a_{pl} = a_{01}(2p+|l|)\ . \tag{55}$$

2.3 The family q=1

In the following we will restrict our analysis to the case in which only the two degenerate modes with $p = 0$ and $l = \pm 1$ belonging to family $q = 1$ are active. This situation can be simply realized experimentally by a) putting a small absorbing dot on the laser axis to suppress the modes with $l = 0$ and b) arranging that the size of the active region is on the order of some beam waists to keep the laser below the activation threshold of higher order modes. Actually, in our numerical simulations we always checked the validity of this assumption by including in the dynamical equations also the modes $p = 0$, $l = \pm 2$; $p = 1$, $l = \pm 1$ and $p = 0$, $l = 3$. In all cases we verified that the intensities of such modes were at least two orders of magnitudes smaller than the intensities of the modes of family $q = 1$.

If the only relevant modes are those belonging to family $q = 1$, the slowly varying envelope of the electric field F can be written as

$$F(\rho, \varphi, \tau) = A_1(\rho, \varphi) f_1(\tau) + A_2(\rho, \varphi) f_2(\tau) \tag{56}$$

with

$$A_1(\rho, \varphi) = \frac{2}{\sqrt{\pi}} \rho e^{-\rho^2} e^{i\varphi} \tag{57}$$

$$A_2(\rho, \varphi) = \frac{2}{\sqrt{\pi}} \rho e^{-\rho^2} e^{-i\varphi} \tag{58}$$

or equivalently

$$F(\rho, \varphi, z) = B_1(\rho, \varphi) g_1(\tau) + B_2(\rho, \varphi) g_2(\tau) \tag{59}$$

with

$$B_1(\rho, \varphi) = \sqrt{\frac{2}{\pi}} 2\rho e^{-\rho^2} \cos\varphi \tag{60}$$

$$B_2(\rho, \varphi) = \sqrt{\frac{2}{\pi}} 2\rho e^{-\rho^2} \sin\varphi \, . \tag{61}$$

The functions A_1 and A_2 represent the two doughnut modes with opposite helicity but equal intensity distribution in the transverse plane (Fig. 3). The functions B_1 and B_2 (TEM_{10} and TEM_{01} modes) are linear combinations of the previous ones and show two intensity peaks on the x and the y axis, respectively (Figs. 4a,b). By choosing the reference frequency as $\omega_0 = \omega_{\overline{m}01} + k\alpha$ the equations for the modal amplitudes can be cast in the form

$$\frac{df_i}{d\tau} = -(1 - i\alpha) \left[f_i - 2C \int_0^{2\pi} d\varphi \int_0^{\infty} d\rho\rho \, A_i^* F D \right] \qquad i = 1, 2, \tag{62}$$

$$\frac{dg_i}{d\tau} = -(1 - i\alpha) \left[g_i - 2C \int_0^{2\pi} d\varphi \int_0^{\infty} d\rho\rho \, B_i F D \right] \qquad i = 1, 2. \tag{63}$$

3 Cylindrical active region

We consider first the case in which the active region has a perfect cylindrical symmetry and the function χ_V depends only on the radial coordinate ρ

$$\chi_V(\rho) = \begin{cases} 1 & \rho \leq \psi/2 \\ 0 & \rho > \psi/2 \end{cases} \tag{64}$$

where $\psi = d_A/w_0$ is the normalized diameter of a circular section of the active region. Two kinds of stationary solutions exist, the doughnut solution

$$F^{st} = A_i f_i^{st} \qquad i = 1 \quad \text{or} \quad i = 2 \tag{65}$$

and the two-peak solutions

$$F^{st} = B_1 g_1^{st} + B_2 g_2^{st} \, . \tag{66}$$

The coefficients g_1^{st} and g_2^{st} are assumed to be real, so that Eq. (66) represents a TEM_{10} mode rotated by an angle $\theta = \tan^{-1}(g_1^{st}/g_2^{st})$ (see Fig. 5c). Due to the cylindrical symmetry of the system any value of θ is allowed.

The threshold value $2C_{thr}$ for the pump parameter is identical for both kinds of solutions and it explicitly reads

$$2C_{thr} = \left[1 - \mathrm{e}^{-\psi^2/2}(1 + \psi^2/2)\right]^{-1} \, . \tag{67}$$

In the limit of active region much larger than the area occupied by the beam ($\psi \to \infty$) one has $2C_{thr} \to 1$.

3.1 Stability of the doughnut solution

The linear stability analysis of the stationary solutions can be considerably simplified in the limit $|F|^2 \ll 1$, valid for a laser operating near threshold.

In the case of the doughnut solution we consider, for definiteness, the solution $F^{st} = A_1 f_1^{st}$ and study its stability against the growth of the other doughnut mode. The characteristic equation for the eigenvalue λ of the linearized system is

$$\lambda^2 + \gamma\lambda + \beta\gamma(1 - \mathrm{i}\alpha) = 0 \tag{68}$$

where β is defined as

$$\beta = \frac{2C}{2C_{thr}} - 1 \, . \tag{69}$$

The solutions of Eq. (68) are strongly dependent on the term α. We consider separately the case $\alpha = 0$ and the case $\alpha \neq 0$.

$\alpha = 0$. As mentioned in Sec. 2, this situation is not realistic for a semiconductor laser but it describes a perfectly tuned Class-B laser, like a CO_2 laser. The solutions of Eq. (68) are

$$\lambda_\pm = \frac{1}{2}\left[-\gamma \pm \sqrt{\gamma^2 - 4\beta\gamma}\right] \tag{70}$$

and their real parts are always less than zero. The doughnut solution is stable in a tuned Class-B laser with cylindrical symmetry. This is a well-known result, which extends to all kinds of lasers that can be described by the Maxwell-Bloch equations for two-level atoms.

$\alpha \neq 0$. In this case the eigenvalues $\lambda_\pm$ are complex numbers with

$$\mathcal{R}e\ \lambda_\pm = \frac{\gamma}{2}\left\{-1 \pm \frac{1}{\sqrt{2}}\left[\sqrt{\left(1-\frac{4\beta}{\gamma}\right)^2 + \left(\frac{4\beta\alpha}{\gamma}\right)^2} + 1 - \frac{4\beta}{\gamma}\right]^{1/2}\right\} \tag{71}$$

and

$$\mathcal{I}m\ \lambda_\pm = \pm\frac{\gamma}{2\sqrt{2}}\left[\sqrt{\left(1-\frac{4\beta}{\gamma}\right)^2 + \left(\frac{4\beta\alpha}{\gamma}\right)^2} - 1 + \frac{4\beta}{\gamma}\right]^{1/2} . \tag{72}$$

The instability condition $\mathcal{R}e\ \lambda_+ > 0$ is fulfilled when

$$\beta > \beta_1 = \frac{\gamma}{\alpha^2} \tag{73}$$

and the frequency of the periodic solution which arises from this bifurcation is

$$\omega_1 = \sqrt{\gamma\beta_1} = \frac{\gamma}{\alpha} . \tag{74}$$

Since γ is always much smaller than 1 in semiconductor lasers and α ranges from 4 to 6 [17], it follows from Eq. (73) that the stability domain for the doughnut solutions in a very narrow region just above threshold.

A remarkable feature of the above analysis is that the geometry of the laser (i.e. the shape of the function χ_V) affects only the value of the lasing threshold $2C_{thr}$, but not the stability properties of the doughnut solution, because Eq. (68) depends only on the scaled quantity β. Hence, the results of this analysis can be extended to any laser geometry.

3.2 Stability of the two-peak solutions

This kind of solutions are always unstable in a perfectly tuned Class-B laser with cylindrical symmetry. Yet, the analysis of the previous subsection proved that the linewidth enhancement factor α changes the stability properties of the doughnut solutions. We expect strong effects also on the stability of the two-peak solutions.

The linear stability analysis of the two-peak solution (66) in the limit $|F|^2 \ll 1$ yields to the following characteristic equation

$$\lambda^2 + \lambda\left(\gamma - \frac{4}{3}\beta\right) - \frac{2}{3}\gamma\beta + \frac{4}{9}(1+\alpha^2)\beta^2 = 0 , \tag{75}$$

where, because of the cylindrical symmetry of the system, the angle θ does not appear. Again, we treat separately the case $\alpha = 0$ and the case $\alpha \neq 0$.

$\alpha = 0$. The solutions of Eq. (75) are

$$\lambda_1 = \frac{2}{3}\beta , \qquad \lambda_2 = \frac{2}{3}\beta - \gamma \tag{76}$$

and λ_1 is always positive above threshold, as expected.

$\alpha \neq 0$. In this case we have

$$\lambda_{\pm} = \frac{1}{2}\left[\frac{4}{3}\beta - \gamma \pm \sqrt{\gamma^2 - \frac{16}{9}\alpha^2\beta^2}\right] . \tag{77}$$

If $\alpha < 1$ the real part of at least one eigenvalue is positive and the solution is unstable for every value of β and γ.
For $\alpha > 1$ the solution is stable in the interval $\beta_2 < \beta < \beta_3$ with

$$\beta_2 = \frac{3}{2}\frac{\gamma}{1+\alpha^2} \tag{78}$$

and

$$\beta_3 = \frac{3}{4}\gamma . \tag{79}$$

It must be noted that the two boundaries of stability $\beta = \beta_2$ and $\beta = \beta_3$ have different properties. At $\beta = \beta_2$ the *real* eigenvalue λ_+ changes its sign, leading to a steady-state instability. On the contrary, $\beta = \beta_3$ is the boundary of a Hopf bifurcation, characterized by the frequency

$$\omega_2 = \frac{\gamma}{2}\sqrt{\alpha^2 - 1} . \tag{80}$$

It is worth noting that both ω_1 and ω_2 scales as γ with coefficient of proportionality depending only on α. On the contrary, the relaxation oscillations in semiconductor lasers scale as $\sqrt{\gamma}$ [25]. We can conclude that the dynamical frequencies ω_1 and ω_2 are not connected with relaxation processes but they are a consequence of the amplitude-phase coupling induced by the factor α.

3.3 General stability scenario

If $1 < \alpha < \sqrt{2}$ the stability domains of the doughnut and two-peak solutions have a common domain ($\beta_2 < \beta < \beta_1$), leading to multistability among these stationary solutions. Such values of α are too small for real semiconductor lasers but the correspondence between semiconductor laser and detuned Class-B lasers suggests that multistability can be observed, for instance, in CO_2 lasers.

More interesting for the purposes of the present work is the case $\alpha > \sqrt{2}$. In this situation the chain of inequalities $\beta_1 < \beta_2 < \beta_3$ holds and we can distinguish four different regions

a) $0 < \beta < \beta_1$: only the two doughnut solutions are stable; there is bistability between them

b) $\beta_1 < \beta < \beta_2$: all kinds of stationary solutions are unstable and the laser reaches a dynamical regime in which the two doughnut modes beat with the frequency ω_1 of the Hopf bifurcation which occurs at $\beta = \beta_1$

c) $\beta_2 < \beta < \beta_3$: only the two-peak solutions are stable; there is an infinite number of stable states, one for each possible orientation of the pattern in the transverse plane

d) $\beta > \beta_3$: as in region b) all stationary solutions are unstable, but now the dynamics is characterized by the beating of modes TEM_{10} and TEM_{01} with the frequency ω_2 arising from the Hopf bifurcation at $\beta = \beta_3$

This situation is described schematically in Fig. 5. The numerical integration of the dynamical equations fully confirmed this picture. The parameters adopted in the simulations were $\gamma = 1/30$, $\alpha = 4$, $\psi = 4$. With such choice of the parameters we have $\beta_1 = 0.00208$, $\beta_2 = 0.0029$, $\beta_3 = 0.025$.

In regions a) and c) we always found the doughnut and the two-peak solutions, respectively, and we verified that the orientation of the peaks in region c) depends only on the initial conditions. The power spectra $S(\omega/\gamma)$ in region b) and d) have been obtained with $\beta = 0.0022$ and $\beta = 0.026$, respectively. The dominant frequencies are close to the values $\omega_1/\gamma = 0.25$ and $\omega_2/\gamma \simeq 1.94$ obtained from Eqs. (74) and (80) for $\alpha = 4$. The discrepancies are within 10% and they are probably due to the nonlinear interaction between the modes.

4 Square active region

From the viewpoint of possible applications the only interesting regions are a) and c), where the laser emits a continuous wave. In particular, region a) is characterized by bistability between the two doughnut configurations, while in region c) all orientations of the two-peak patterns are equivalent.

As far as the use of the laser as an optical switching device is concerned, bistability between two states with clearly different properties (the behaviour of the phase for doughnut modes) is much preferable to the multistability present in region c). Actually, optical switching between doughnut modes with opposite helicity has been already observed in a He-Ne laser (Class-A laser) [12].

Unfortunately, the stability analysis of Section 3.1 showed that the width of region a) is so small to make rather infeasible an experiment of switching involving doughnut modes in a semiconductor laser. Region c) is wider, but in this case the cylindrical symmetry of the laser leads to multistability among a continuous set of stationary states.

This problem can be overcome by considering a different geometry for the laser, namely a square active region or a square filter [16]. In this situation we expect that only two among all possible orientations of the two-peak structure are privileged, and precisely the two orthogonal directions corresponding to the diagonals of the square.

In this section we will adopt cartesian coordinates x and y so that the modal functions A_i and B_i take the form

$$A_1(x,y) = \frac{2}{\sqrt{\pi}}\,(x+\mathrm{i}y)\,\mathrm{e}^{-(x^2+y^2)}\,, \tag{81}$$

$$A_2(x,y) = \frac{2}{\sqrt{\pi}}\,(x-\mathrm{i}y)\,\mathrm{e}^{-(x^2+y^2)}\,, \tag{82}$$

$$B_1(x,y) = \sqrt{\frac{2}{\pi}}\,2x\,\mathrm{e}^{-(x^2+y^2)}\,, \tag{83}$$

$$B_2(x,y) = \sqrt{\frac{2}{\pi}}\,2y\,\mathrm{e}^{-(x^2+y^2)}\,. \tag{84}$$

We assume that the sides of the square are parallel to the x and y axes so that the function χ_V is now defined as

$$\chi_V(x,y) = \begin{cases} 1 & |x|,|y| \leq \psi/2 \\ 0 & |x|,|y| > \psi/2 \end{cases} \tag{85}$$

where $\psi = l_A/w_0$ is the normalized length of the side of the square.

First of all we observe that, while the doughnut solution is still a stationary solution although the system has lost the cylindrical symmetry, for what concerns the two-peak solutions the square symmetry removes the rotational degeneracy and only the solutions with peaks located on the axes or on the diagonals of the square survive.

The threshold for all these stationary solutions is the same and of course it differs from the one obtained in the cylindrical case. We have now

$$2C_{thr} = \left\{ \mathrm{erf}\left(\frac{\psi}{\sqrt{2}}\right) \left[\mathrm{erf}\left(\frac{\psi}{\sqrt{2}}\right) - \sqrt{\frac{2}{\pi}} \mathrm{e}^{-\psi^2/2} \psi \right] \right\}^{-1} , \tag{86}$$

where erf is the error function defined in the usual way. Again $2C_{thr} \to 1$ as $\psi \to \infty$.

4.1 Stability of the doughnut solution

As stated in Sec. 3.1 the stability properties of this kind of solution are completely independent from the shape of the active region. The instability condition (73) is still valid, provided the expression (86) for $2C_{thr}$ is replaced in the definition of the parameter β.

4.2 Stability of the two-peak solutions

The square shape of the active region selects as stationary solutions only the ones for which $\theta = n\pi/4$ with $n = 0, 1, 2 \ldots$.
Obvious symmetry considerations suggests dividing such solutions in two classes:
n even: solutions with peaks located on the x and y axes
n odd: solutions with peaks located on the diagonals of the square.

The characteristic equation derived from the linear stability analysis in the usual limit $|F|^2 \ll 1$ is

$$\lambda^3 + \lambda^2[2\beta(S_n - 1) + \gamma] + \lambda[\beta^2(S_n - 1)^2(1 + \alpha^2) + 2\gamma\beta(2S_n - 1)] + \\ \gamma\beta^2(1 + \alpha^2)(S_n - 1)(3S_n - 1) = 0 , \tag{87}$$

where β is defined as in Eq. (69) and S_n is a function of ψ such that

$$S_n(\psi) = \begin{cases} [I_2(\psi)^2] \,/\, [I_0(\psi) I_4(\psi)] & n \text{ even} \\ [I_0(\psi) I_4(\psi) - I_2(\psi)^2] \,/\, [I_0(\psi) I_4(\psi) + 3 I_2(\psi)^2] & n \text{ odd} \end{cases} \tag{88}$$

where

$$I_n(\psi) = \int_{-\psi}^{\psi} dx \, x^n \, \mathrm{e}^{-x^2} . \tag{89}$$

Fig. 6 shows the behaviour of S_n as a function of ψ. Two features are clearly visible
i)

$$S_n(\psi) \begin{cases} \geq 1/3 & \forall\, \psi \qquad n \text{ even} \\ \leq 1/3 & \forall\, \psi \qquad n \text{ odd} \end{cases} \tag{90}$$

ii) $S_n(\psi) \rightarrow 1/3$ as $\psi \rightarrow \infty$.
In this limit there is no distinction between cylindrical and square geometry and Eq. (87) reduces to Eq. (75).

For finite values of ψ the Hurwitz criterion applied to the cubic equation (87) leads to the following results:
a) A necessary condition for the real part of all the eigenvalues to be negative is

$$\mathcal{F}(\alpha) = \frac{2|\alpha|}{\alpha^2 + 4|\alpha| + 1} < S_n(\psi) < 1/3\ . \tag{91}$$

This condition, together with item i) of the previous list, implies that the only stable two-peak solutions are the odd ones. In Fig. 6 the dashed lines represent the function $\mathcal{F}(\alpha)$ for $\alpha = 4$ and $\alpha = 6$. The odd two-peak solutions are stable for values of ψ larger than the intersection points of those lines with the curve S_n, n odd.
b) If condition a) is fulfilled the odd solutions are stable for values of β such that

$$\beta_- < \beta < \beta_+ \tag{92}$$

with

$$\beta_\pm = \frac{\gamma}{2} \frac{S_n(1+\alpha^2) + 2(1-2S_n) \pm \sqrt{{S_n}^2(1+\alpha^2)^2 - 4\alpha^2(1-2S_n)^2}}{(1-S_n)^2(1+\alpha^2)}\ . \tag{93}$$

Summarizing, in the case of a square active region, the only stable two-peak solutions are those placed on the diagonals of the square. The laser shows bistability between two states whose intensity configurations are orthogonal in space. This kind of bistability is completely different from that between doughnut modes, because the doughnut modes have the same intensity configuration and they differ only for the behaviour of the optical phase.

A comparison with the previous section shows that $\beta_2 < \beta_- < \beta_+ < \beta_3$: the stability domain for the two-peak solution is smaller than in the cylindrically symmetric case. Another difference is that now both bifurcations at $\beta = \beta_-$ and $\beta = \beta_+$ are Hopf bifurcations. The frequencies ω_+ and ω_- associated with the two bifurcations are

$$\omega_\pm = \gamma \frac{\left[-2(1-2S_n)^2 + S_n^2(1+\alpha^2) \pm S_n\sqrt{S_n^2(1+\alpha^2)^2 - 4\alpha^2(1-2S_n)^2}\right]^{1/2}}{\sqrt{2}(1-S_n)}\ . \tag{94}$$

However, $\beta_- \rightarrow \beta_2$, $\beta_+ \rightarrow \beta_3$, $\omega_+ \rightarrow \omega_2$ and $\omega_- \rightarrow 0$ as $\psi \rightarrow \infty$, and in this limit we recover exactly the same results as in the previous section.

In conclusion, we have the same stability scenario as in Fig. 5, apart from the reduced size of the stability domain of the two-peak solutions and the disappearance of the rotational degeneracy for this solution.

5 Conclusions

Our analysis shows that, most commonly, the laser considered here develops dynamical oscillations in which the two doughnut modes, or the two TEM_{10} and TEM_{01} modes, exchange their energy. However, we identified two distinct regions in the parameter space, where stable stationary states exist and this feature can be utilized for applicative purposes.

In the first of these regions there is bistability between the doughnut states, so that one can expect a switching behaviour of the type described in [12]. However, this bistability domain seems very small in the parameter space.

In the second region there is a stable two-peak stationary state with a TEM_{10} configuration and, similarly, all the steady states obtained from this by an arbitrary rotation around the laser axis are stable when the system is cylindrically symmetric; an initial random fluctuation determines the angular orientation of the state. This infinite degeneration of the stationary state under rotation seems detrimental for practical applications such as, for example, switching. However we have shown that if the active region has a square instead of a circular section, in this regime the system always approaches one of the two stationary states, in which the two peaks are located along the two diagonals of the square. In the future, we plan to study the switching behaviour of the laser in this bistable configuration, and also to explore the possibility of realizing optical gate operations.

Acknowledgement – We thank Dott. F. Castelli for useful discussions. This work has been carried out in the framework of the ESPRIT Basic Research Project 7118 TONICS, of the Collaborative NATO Research Grant 92.01369.CT02 and of the CNR Grant 93.0008 04.PF71 (Progetto Finalizzato Telecomunicazioni).

Appendix - Comparison with two-level Class-B lasers

In this appendix we demonstrate that the dynamical equations for a semiconductor laser (51-52) are formally identical to the equations for a two-level Class-B laser, where the linewidth enhancement factor α is replaced by the atomic detuning Δ.
The equations for a two-level laser are [24]

$$\frac{df_{pl}}{dt} = -k\left[(1+\mathrm{i}a_{pl})f_{pl} - 2C\int_0^{2\pi}d\varphi\int_0^{\infty}d\rho\rho\; A_{pl}^{*}\,P\right] \tag{95}$$

$$\frac{\partial P}{\partial t} = \gamma_{\perp}\left[FD-(1+\mathrm{i}\Delta)P\right] \tag{96}$$

$$\frac{\partial D}{\partial t} = -\gamma_{\|}\left[\frac{1}{2}(F^{*}P+FP^{*})-\chi_V\right] \tag{97}$$

where $k, \gamma_{\perp}, \gamma_{\|}$ are the decay rates of the electric field, the atomic polarization and the difference of population between the two levels, respectively. A Class-B laser is characterized by the conditions

$$\gamma_{\|} \ll k \ll \gamma_{\perp} \tag{98}$$

which allow for the adiabatic elimination of the atomic polarization P, so that one obtains

$$\frac{df_{pl}}{dt} = -k\left[(1+\mathrm{i}a_{pl})f_{pl} - 2C\frac{1-\mathrm{i}\Delta}{1+\Delta^2}\int_0^{2\pi}d\varphi\int_0^{\infty}d\rho\rho\; A_{pl}^{*}\,D\,F\right] \tag{99}$$

$$\frac{\partial D}{\partial t} = -\gamma_{\|}\left[D\left(1+\frac{|F|^2}{1+\Delta^2}\right)-\chi_V\right]\,. \tag{100}$$

With the substitutions

$$\frac{f_{pl}}{\sqrt{1+\Delta^2}} \longrightarrow f_{pl}, \qquad \frac{F}{\sqrt{1+\Delta^2}} \longrightarrow F, \qquad \frac{2C}{1+\Delta^2} \longrightarrow 2C, \qquad \Delta \longrightarrow \alpha \tag{101}$$

and the definitions

$$\tau = kt, \qquad \gamma = \gamma_{\|}/k \tag{102}$$

Eqs. (99-100) become identical to Eqs. (51-52).

References

1. N. B. Abraham and W. J. Firth, *Overview of transverse effects in nonlinear-optical systems*, J. Opt. Soc. Am. B **7**, 951-962 (1990)

2. L. A. Lugiato, *Spatio-temporal structures. Part I*, Phys. Rep. **219**, 293-310 (1992)

3. C. O. Weiss, *Spatio-temporal structures. Part II. Vortices and defects in lasers*, Phys. Rep. **219**, 311-328 (1992)

4. J. V. Moloney, H. Adachihara, D. W. McLaughlin and A. C. Newell, *Fixed points and chaotic dynamics of an infinite dimensional map*, in *Chaos, Noise and Fractals*, 137-186 eds. R. Pike and L. A. Lugiato, Hilger, Bristol 1988

5. G. S. McDonald and W. J. Firth, *Spatial solitary-wave optical memory*, J. Opt. Soc. Am. B **7**, 1328 (1990)

6. G. S. McDonald and W. J. Firth, *Switching dynamics of spatial solitary wave pixels*, J. Opt. Soc. Am. B **10**, 1081-1089 (1992)

7. M. Brambilla, L. A. Lugiato, V. Penna, F. Prati, C. Tamm and C. O. Weiss, *Transverse laser patterns II. Variational principle for pattern selection, spatial multistability and laser hydrodynamics*, Phys. Rev. A **43**, 5114-5120 (1991)

8. M. Brambilla, L. A. Lugiato, M. V. Pinna, F. Prati, P. Pagani, P. Vanotti, M. Y. Li and C. O. Weiss, *The laser as nonlinear element for an optical associative memory*, Opt. Comm. **92**, 145-164 (1992)

9. P. Vanotti, P. Pagani, L. A. Lugiato and M. V. Pinna, *All-optical associative memory based on the use of the laser as a nonlinear element*, Opt. Lett. **17**, 1526-1528 (1992)

10. S. A. Akhmanov, M. A. Vorontsov, V. Yu. Ivanov, A. V. Larichev and N. I. Zheleznykh, *Controlling transverse-wave interactions in nonlinear optics: generation and interaction of spatiotemporal structures*, J. Opt. Soc. Am. B **9**, 78-90 (1992)

11. M. A. Vorontsov and E. V. Degtyarev, preprint

12. C. P. Smith, Y. Dihardja, C. O. Weiss, L. A. Lugiato, F. Prati and P. Vanotti, *Low energy switching of laser doughnut modes and pattern recognition*, Opt. Comm. **102**, 505-514 (1993)

13. K. Iga, F. Koyama and S. Kinoshita, *Surface Emitting Semiconductors*, IEEE Journal of Quantum Electronics **24**, 1845-1855 (1988)

14. C. J. Chang-Hasnain, M. Orenstein, A. Von Lehemen, L. T. Florez, J. P. Harbison and N. G. Stoffel, *Transverse mode characteristics of vertical cavity surface emitting lasers*, Appl. Phys. Lett. **57**, 218-220 (1990)

15. J. L. Jewell, Y. H. Lee, A. Scherer, S. L. McCall, N. A. Olsson, R. S. Tucker, C. A. Burrus, J. P. Harbison, L. T. Florez, A. C. Gossard and J. H. English, *Nonlinear FP etalons and microlaser devices*, in *Digital Optical Computing*, 44-66 SPIE Vol. CR35, 1990

16. H. Li, T. L. Lucas, J. McInerney and R. A. Morgan, *Transverse Modes and Patterns of Electrically Pumped Vertical Cavity Surface Emitting Semiconductor Lasers*, Chaos, Noise and Fractals, same volume as this paper

17. C. H. Henry, *Theory of the Linewidth of Semiconductor Lasers*, IEEE Journal of Quantum Electronics **QE-18**, 259-264 (1982)

18. G. P. Agrawal and N. K. Dutta, *Long-wavelength semiconductor lasers* Van Nostrand Reinhold, New York, 1986

19. H. Adachihara, O. Hess, E. Abraham, P. Ru and J. V. Moloney, *Spatiotemporal chaos in broad-area semiconductor lasers*, J. Opt. Soc. Am. B **10**, 658 (1993)

20. D. Marcuse, *Gaussian approximation of the fundamental modes of graded-index fibers*, J. Opt. Soc. Am. **68**, 103-109 (1978)

21. H. Kogelnik, *On the Propagation of Gaussian Beams of Light Through Lenslike Media Including those with a Loss or Gain Variation*, Appl. Opt. **4**, 1562-1569 (1965)

22. G. P. Agrawal, *Population pulsation and nondegenerate four-wave mixing in semiconductor lasers and amplifiers*, J. Opt. Soc. Am. B **5** 147-158 (1988)

23. H. Kogelnik and T. Li, *Laser Beams and Resonators*, Appl. Opt. **5**, 1550-1567 (1966)

24. L. A. Lugiato, G.-L. Oppo, J. R. Tredicce, L. M. Narducci and M. A. Pernigo, *Instability and spatial complexity in a laser*, J. Opt. Soc. Am. B **7**, 1019-1033 (1990)

25. D. E. McCumber, *Intensity Fluctuations in the Output of cw Laser Oscillator I.*, Phys. Rev. **141**, 306-322 (1966)

Figure captions

Fig. 1 Lateral view of the SEL: L is the distance between the two facets, L_A is the width of the active region, d is the diameter of a circular section of the cylinder.

Fig. 2 Transverse sections of the SEL: a) circular active region of diameter d_A, b) square active region of size l_A.

Fig. 3 Intensity distribution in the transverse plane for the doughnut modes A_1 and A_2.

Fig. 4 Intensity distribution in the transverse plane for the modes B_1 (a) and B_2 (b).

Fig. 5 Scheme of the four domains discussed in the text: a) the two doughnuts are stable, b) the laser shows undamped oscillations at a frequency close to ω_1, c) the two-peak solutions with arbitrary orientation θ are stable, d) the laser shows undamped oscillations at a frequency close to ω_2.

Fig. 6 Plot of the function $S_n(\psi)$ for odd and even values of the integer n. The asymptotic value $1/3$ and the values of the function $\mathcal{F}(\alpha)$ for $\alpha = 4$ and $\alpha = 6$ are represented by the dashed lines.

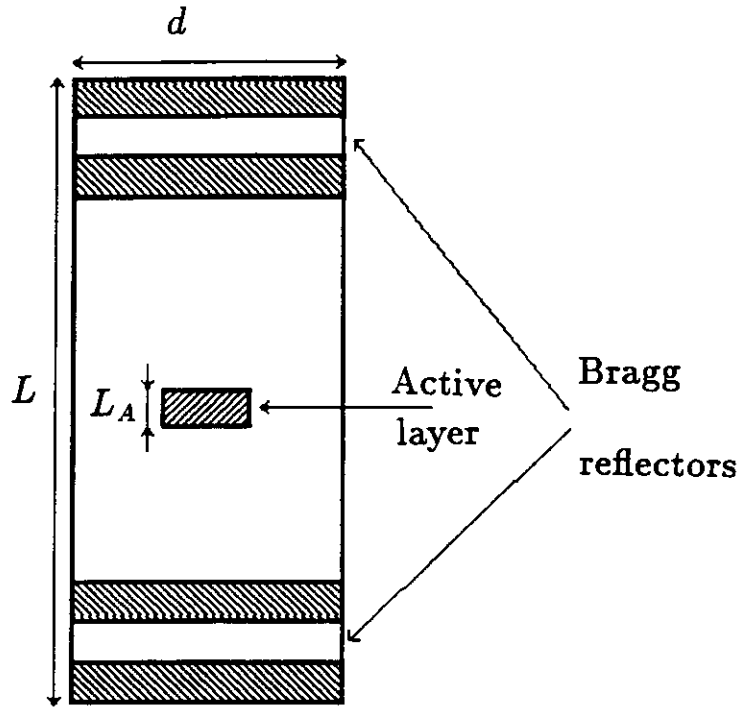

Fig 1

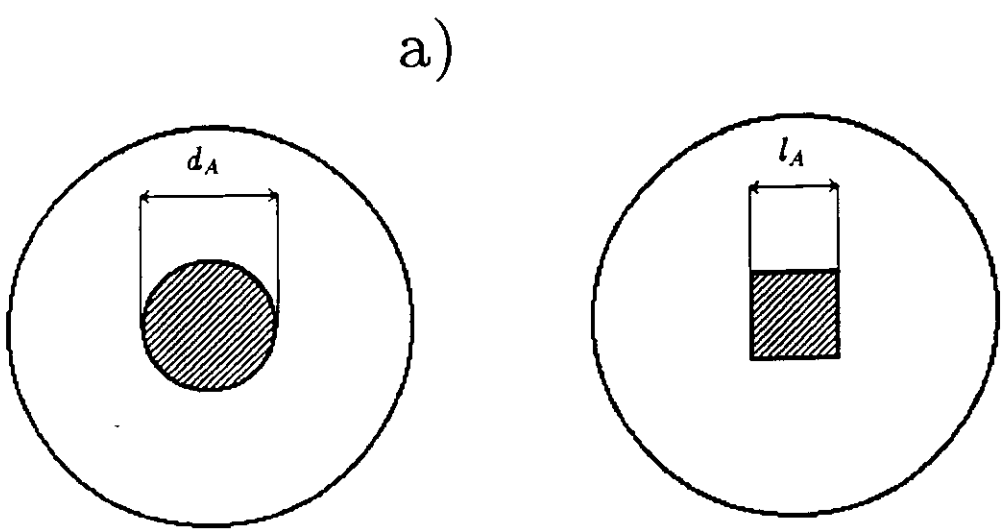

Fig 2

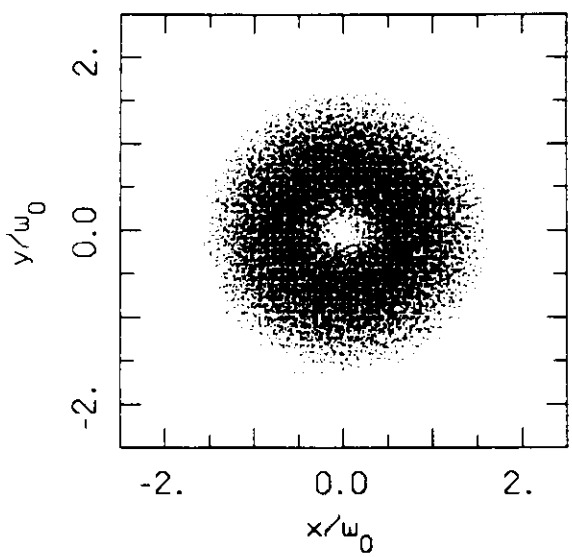

Fig. 3

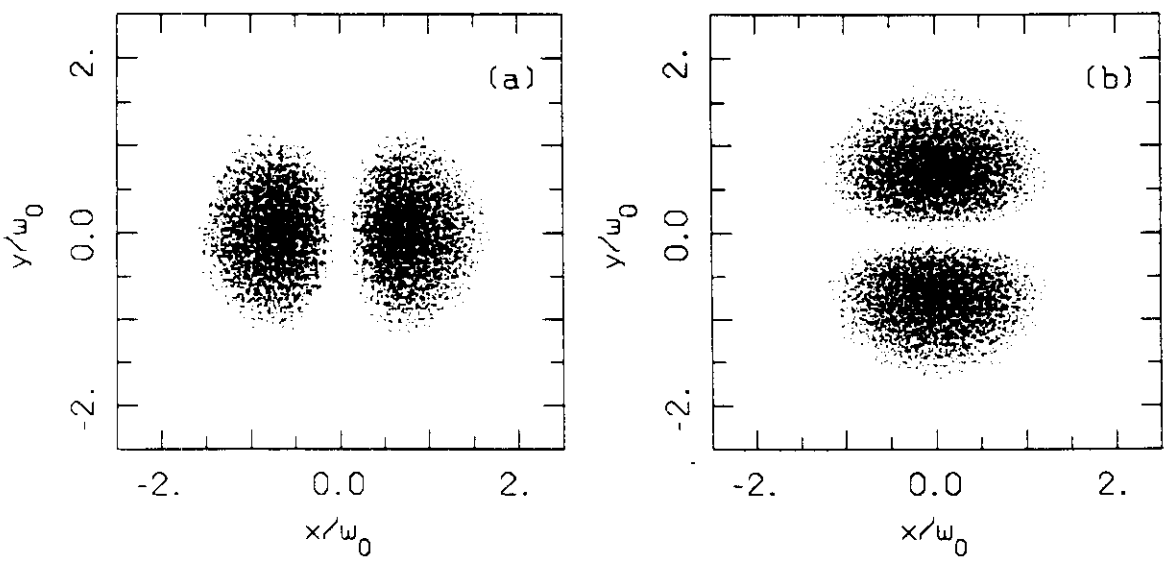

Fig. 4

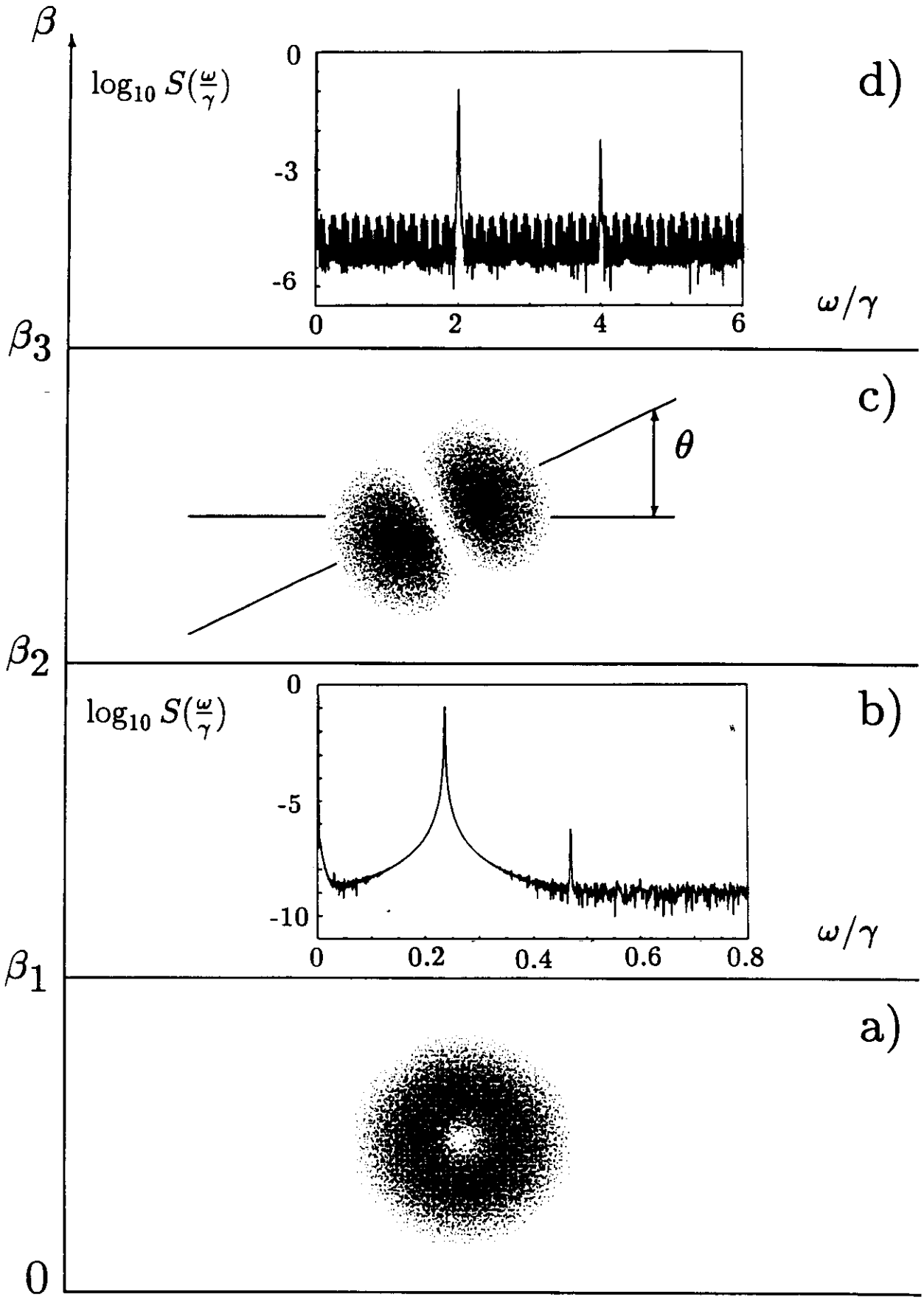
β
log10 S(ω/γ)
0
-3
-6
0
2
4
6
ω/γ
d)
β3
c)
θ
β2
log10 S(ω/γ)
0
-5
-10
0
0.2
0.4
0.6
0.8
ω/γ
b)
β1
a)
0

25 Fig 5

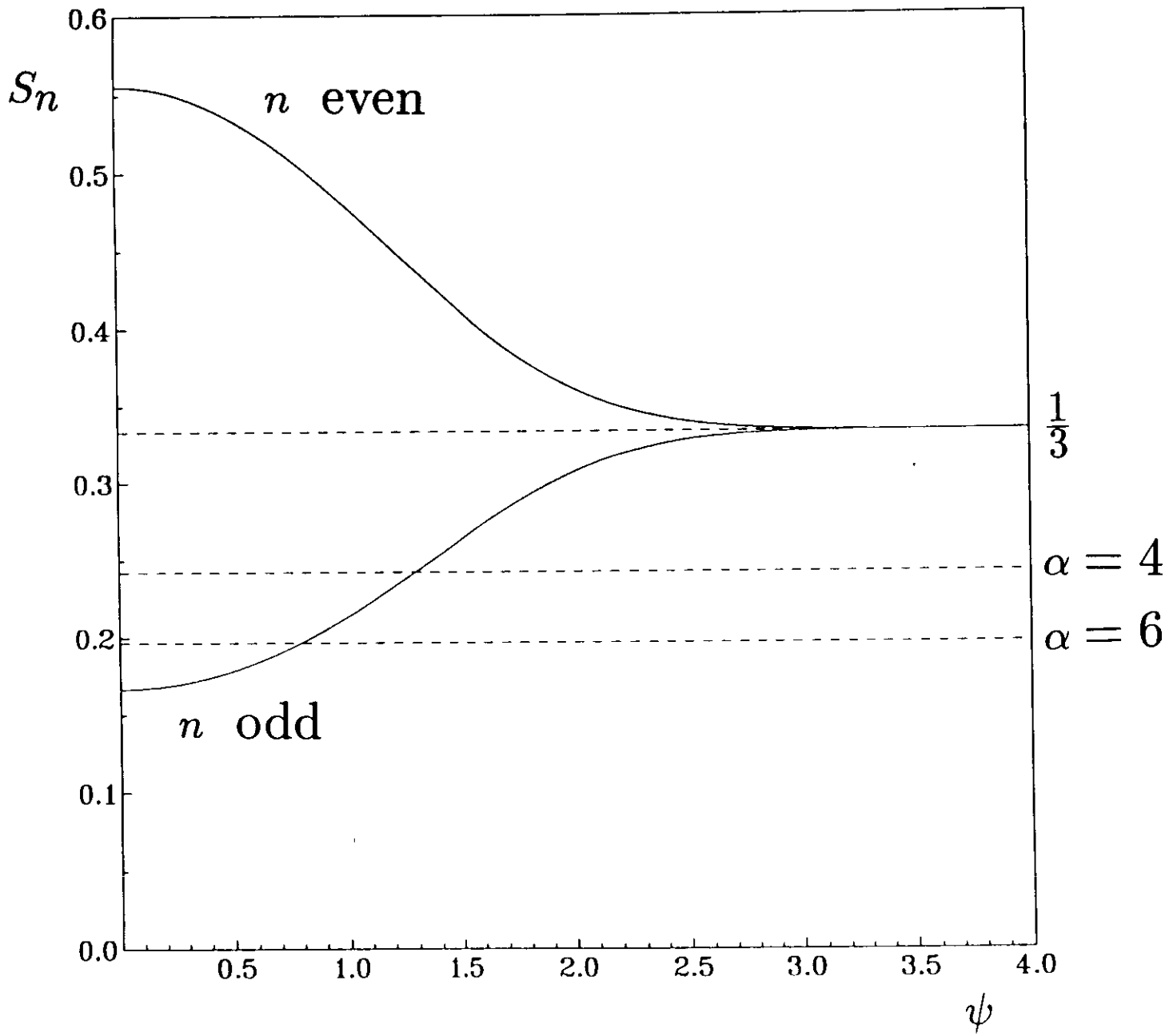
S_n
n even
n odd
$\frac{1}{3}$
$\alpha = 4$
$\alpha = 6$
0.6
0.5
0.4
0.3
0.2
0.1
0.0
0.5
1.0
1.5
2.0
2.5
3.0
3.5
4.0
ψ

Fig 6